Low-Frequency Oscillations Analysis in AC Railway Networks Using Eigenmode Identification

Paul Frutos*, Juan Manuel Guerrero*, Iker Muniategui†, Iban Vicente†, Aitor Endemano†, and Fernando Briz*
*University of Oviedo, Department of Electrical, Computer & System Engineering, Gijón, Spain
Email: frutospaul@uniovi.es, guerrero@uniovi.es, fbriz@uniovi.es
† Ingeteam Power Technology S.A., Traction R&D, Zamudio, Spain
Email: iker.muniategui@ingeteam.com, iban.vicente@ingeteam.com, aitor.endemano@ingeteam.com

***Abstract*—Dynamic interactions among AC railway networks and train power converters have been reported to cause low-frequency oscillations (LFO) and eventually instability phenomena, which can collapse the railway power system. Several system parameters can influence in the appearance of LFO, including catenary length, power consumption, control bandwidths, etc. This paper proposes a methodology for the analysis and understanding of the impact of all these parameters on the LFO. The proposed method combines time-domain simulations with eigenvalue analysis. Eigenvalue migration will be shown to be a powerful tool to understand the risk of instability and to analyse potential remedial actions.**

I. Introduction

Modern train railway systems include a large number of power electronic converters, aimed to improve performance and efficiency. Despite the benefits, complex dynamic interactions among the railway network and the controlled power converters can produce undesired phenomena, which might result in power system instability, including LFO phenomena [1]–[7] and and harmonic instability [8]

LFO phenomena have been reported worldwide for different types of railway networks under different operating conditions (see Table I).

TABLE I: LFO reported cases

N °	Case	$f_0[Hz]$	$f_{osc}[Hz]$	Time
1	Zürich, Switzerland [5]	16.67	5	1995
2	Norway [3]	16.67	1.6	2007
3	Washington, USA [9]	25	3	2006
4	Thionville, France [4]	50	5	2008
5	Siemens test, Germany [1]	50	7	2006
6	Hudong Depot, China [6]	50	2-4	2008
7	Shanhaiguan Hub, China [7]	50	6-7	2011

Reported events include 16,6 Hz catenaries fed from rotary converters [3], and static frequency converters [5], as well as 50 Hz catenaries fed from the grid [4]. Therefore, this paper consider the phenomena occurred when the low-frequency dynamics are mainly determined by the train vehicle.

There is a number of constructive and operational aspects that will affect LFO formation, including catenary line length, consumed power, design and tuning of train catenary-side converter controllers (bandwidth of current and voltage controllers, PLLs, SOGI, etc), interference from other trains, etc [5]. It is not trivial therefore to determine the circumstances in which LFO will occur.

In this paper, modes of operation (i.e. eigenmodes) that can produce LFO are first obtained by means of time-domain simulations, system dynamics being characterized using eigenvalues estimation techniques. Sensitivity is then studied by means of eigenvalue migration analysis. System parameters considered for the analysis presented in this paper include: catenary length; power consumption; characteristics of on-board catenary side converter: current and dc voltage control bandwidths, SOGI, PLL; leakage inductance of the transformer; and dc-link capacitor.

The paper is organized as follows. Section II describes rail-network model used for the study. Section III deals with LFO description and modelling; section IV addresses eigenvalue migration and sensitivity analysis. Finally, conclusions are drawn in section V.

II. Train-network control system model

A simplified representation of the railway system is shown in Fig.1, it is seen to consist of three main elements: power source, transmission line (i.e. catenary line), and power load (i.e. train). For the study of LFO, an equivalent circuit of the transmission line with only resistance and inductance is widely used [1], [5], [6], as capacitive effects can be safely neglected. Fig.2 shows the rail-network model, including control loops, that will be used in this study. The main elements interfacing the network and the traction inverters are the transformer, single-phase four-quadrant power converter (4QC), and DC-link capacitor. The traction inverter is represented as an equivalent linear load in Fig.2.

A cascaded control structure consisting of an outer voltage control loop and an inner current control loop is used to regulate the DC link voltage v_{dc} [9]. The control in Fig.2 operates in dq coordinates, the d-axis voltage cotrrespoding to the catenary voltage. A second order generalized integrator (SOGI) is being used to obtain the quadrature signals. A PLL is used to obtain the grid voltage phase angle θ required for the coordinate transformations to the synchronous reference frame [7].

In order to get the desired current control bandwidth (BW_{cc}) and the voltage control bandwidth (BW_{vc}), controllers (i.e Kp_{cc},Ki_{cc},Kp_{vc},Ki_{vc}) were tuned using the zero-pole cancellation as described in [10]. The design of the PLL was performed according to [11] where the PLL proportional

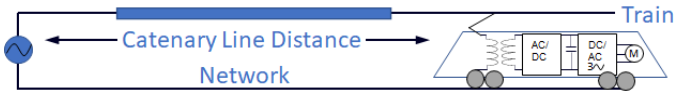

Fig. 1: Simplified representation of the train-network system

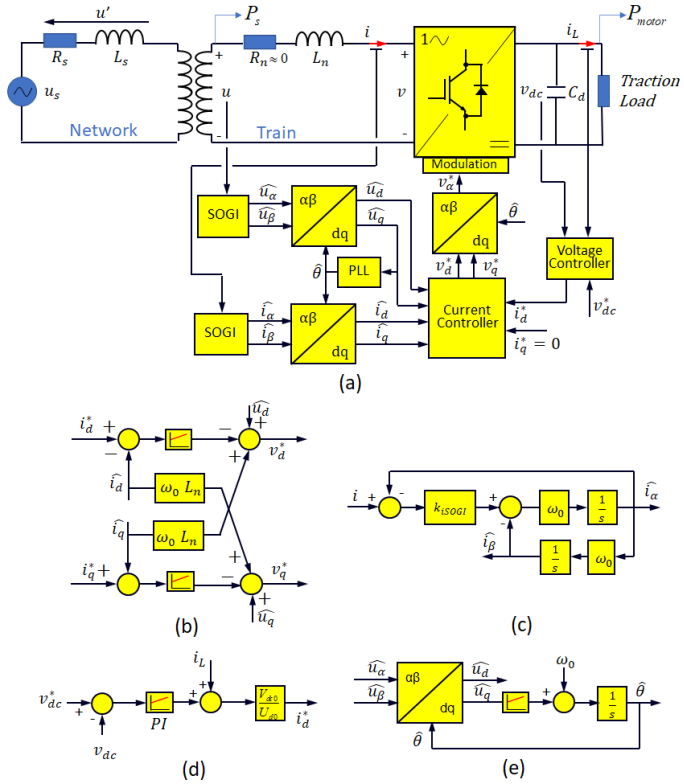

Fig. 2: Rail-network control system model (a) Complete Model (b) Current Controller (c) SOGI (d) DC Voltage Controller (e) PLL

and integral gain are choosen as Kp_{pll}=K_{pll}, Ki_{pll}=$K_{pll}^2/2$. Finally, the value of gain K_{sogi} for second order generalized integrator (SOGI) was chosen as described in [5]

III. LFO MODELING

The typical catenary line voltage and train current waveforms when LFO occur, and its harmonic spectra, are shown in Fig. 3. AC signals in the time domain oscillate at a frequency f_0, their magnitude (envelope) varying at a frequency f_{osc}. The corresponding spectrums show the fundamental component an f_0 escorted by two side bands at $f_L = f_0 - f_{osc}$ and $f_H = f_0 + f_{osc}$ respectively. This behavior can be modelled mathematically as shown by (1).

$$\begin{aligned} u(t) &= U(t)\sin(2\pi f_0 t) \\ &= (U_0 + \Delta U\cos(2\pi f_{osc}t))\sin(2\pi f_0 t) \\ &= U_0\sin(2\pi f_0 t) + \frac{\Delta U}{2}\sin(2\pi f_L t) + \frac{\Delta U}{2}\sin(2\pi f_H t) \end{aligned} \quad (1)$$

It is important to notice that, in general, the magnitude of the harmonic spectra components f_L and f_H are not equal, contrary to equation (1) illustrate. The accurate simulation in Fig.3 shows the actual asymmetry of spectra components. Due to this distortion in the catenary line voltage and vehicle current, the low-frequency oscillations have caused a number of serious issues, such as the malfunction of the protection system, high-voltage, and current that could damage the electrical/electronic equipment, transportation delays, and so on.

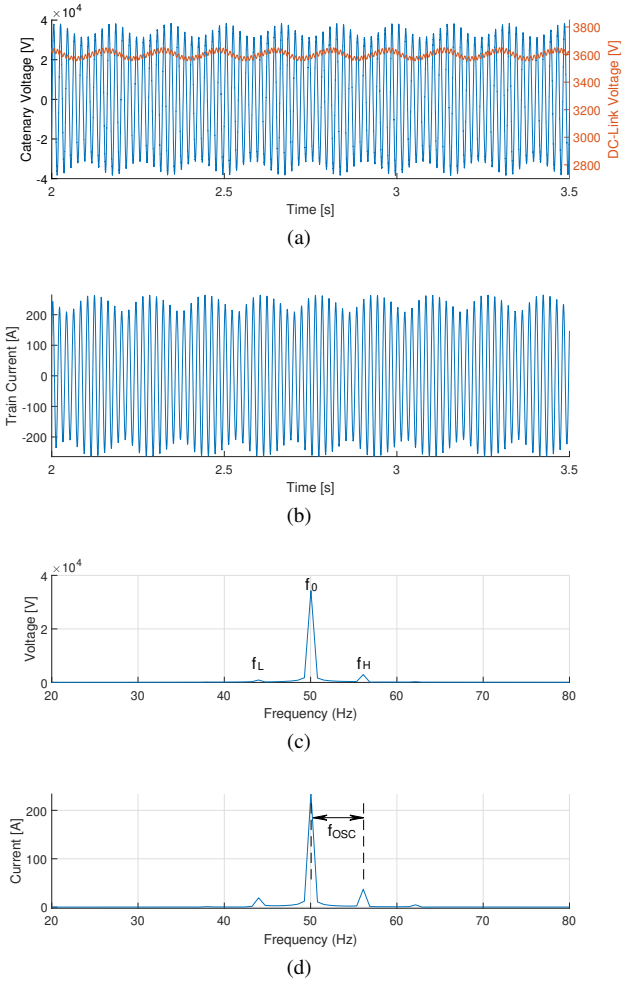

Fig. 3: Simulated LFO phenomena: (a) Catenary Line Voltage and Train DC-Link Voltage (b) Train Current (c) Catenary Line Voltage FFT (d) Train Current FFT

IV. LFO ANALYSIS USING EIGENMODE IDENTIFICATION

In this section eigenmodes are used to characterize the system dynamic behavior when LFO occur. Associated eigenvalues to each eigenmode are obtained by mean of numerical estimation techniques.

The impact on LFO of catenary length and consumed power are first considered. The sensitivity to 4QC control parameters, transformer leakage inductance and dc-link capacitor is then discussed using this approach.

A. Eigenvalue migration due to catenary length

Fig.4 shows the time domain transient response to a disturbance of the dc-link voltage, for different lengths of catenary

line. For this analysis it is considered that 4QC control parameters are constant. The power consumed by the vehicle was only 300 kW. This corresponds to the low power condition reported in [4].

Degradation of dc-link voltage control as the distance increases is readily observed in Fig.4, eventually leading to instability. Transient responses shown in Fig.4 in response to changes in catenary length can modeled as a set of complex conjugates eigenvalues as shown in Fig. 5. The following terms are defined from Fig. 5: ω_n is the natural frequency and σ is the attenuation constant and θ the eigenvalue angle. Using these last two terms, damping ζ ratio and settling time T_s are defined (2). Notice that the damping factor is zero when $\theta = \pi/2$, which is the stability limit.

$$\zeta = \frac{\sigma}{\omega_n} = \cos(\theta) \ , \ T_s = \frac{\ln(0.02)}{\sigma} \tag{2}$$

The trajectory followed by the eigenvalues as the catenary length increases show smaller damping coefficient and slower dynamics, which results in a degradation of the system behavior, eventually becoming unstable.

B. Eigenvalue migration with catenary length and consumed power

Eigenvalue migration with load power is shown in Fig. 6 for three different catenary lengths, short line (20 km), medium line (60 km) and long line (120 km). It is interesting to note that the overall shape of the eigenvalue trajectory is similar for all the three cases. Lower power consumption result in lower damping, i.e. higher instability risks. A closer analysis also reveals that long catenaries combined with low power consumption lead to the highest risk of instability, which is consistent with the behavior reported in the literature [3], [12].

C. Eigenvalue migration with dc-link voltage and current control bandwidths

The influence of the 4QC voltage and current control closed-loop bandwidths is discussed following. For the sake of simplicity, four scenarios are considered for catenary length and power consumption: 1) low distance - low power; 2) low distance - high power; 3) high distance - low power; 4) high distance - high power.

Fig. 7 shows the eigenvalues for different current-control and voltage-control bandwidths for the long-distance catenary - low power consumption case. The general trend is that, for a given current control bandwidth, higher voltage-control bandwidths results in eigenvalue angle θ (as defined in Fig. 5) closer to $\pi/2$ which means shorter damping ratio and larger settling times (σ decreases) and larger natural frequency. On the other hand, it is observed that for a given voltage control bandwidth, larger current-control bandwidths result in larger damping ratio shorter settling times (σ increases), and larger natural frequencies. From Fig. 7 it can be noticed that eigenvalue migration due to simultaneous variation in voltage-control bandwidths and voltage-control bandwidth in this region are close to being orthogonal. It is concluded from Fig. 7 that rather than the bandwidth of the current and voltage control loops, the ratio BWcc/BWv will be critical for system stability.

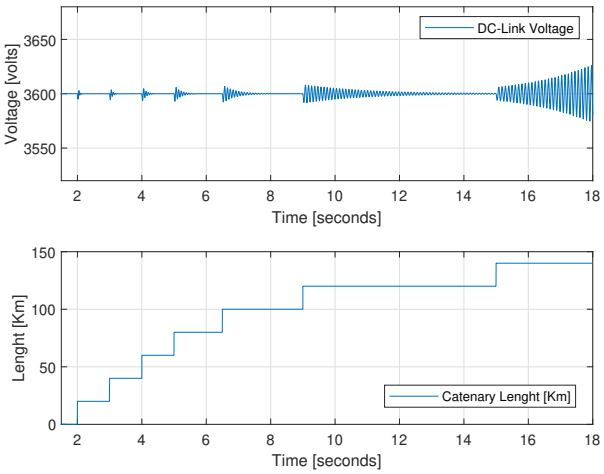

Fig. 4: dc-link time response for variations in catenary-line lenght

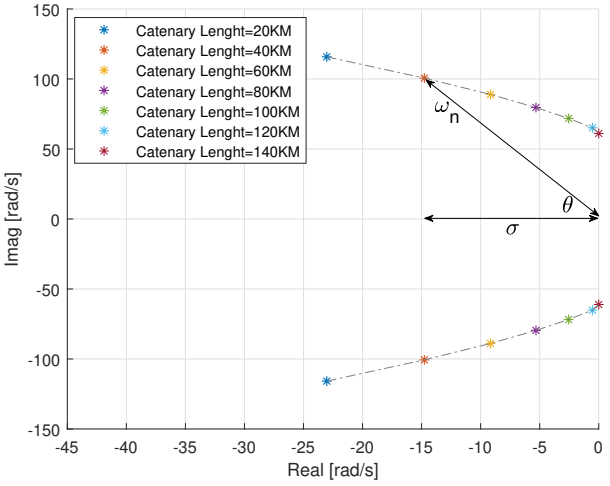

Fig. 5: Eigenvalue migration for variations in catenary-line lenght

Fig. 8 shows the damping ratio, settling time and natural frequency, as a function of BWcc and BWvc, for two different values of the current control bandwidth and the four scenarios discussed at the beginning of this section are considered: 1) low distance - low power; 2) low distance - high power; 3) high distance - low power; 4) high distance - high power. The following conclusions are reached:

- It is observed from Fig.8(a) that the damping ratio (i.e. system stability) always increase as the BWcc/BWvc ratio increases. Low values of the BWcc/BWvc ratio will jeopardize systems stabilty for any operation mode. This trend is independent of the catenary distance and load power.
- From Fig.8(a), in is observed that high distance - low power scenario shows the highest risk of instability (lower

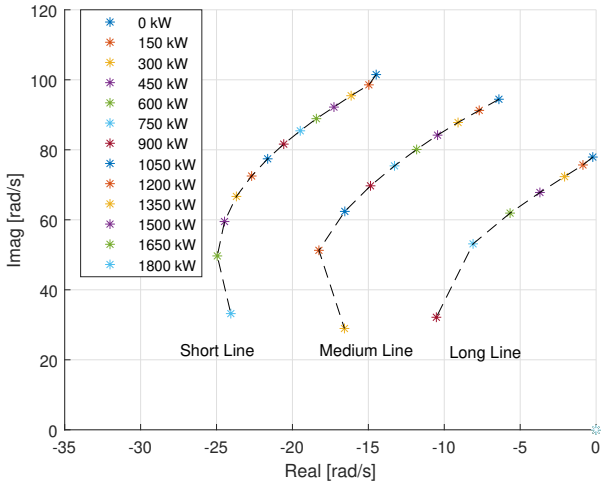

Fig. 6: Eigenvalue migration for variations in load power. Cases: short line (20 km), medium line (60 km) and long line (120) km

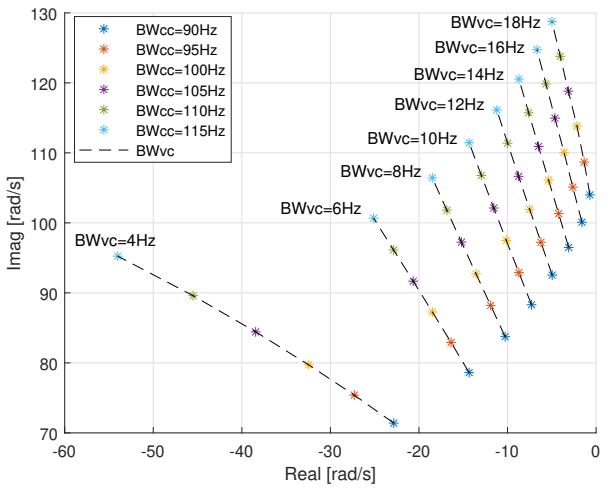

Fig. 7: Eigenvalue migration as a function of dc-link voltage and current control bandwidths, for the case of a long catenary and low power consumption. BWcc and BWvc stand for current and voltage control bandwidths

damping ratio). The damping ratio is seen to change linearly with BWcc/BWvc, independent of BWcc.

- The damping ratio increases when the load power level increases and decreases when the catenary line increases. This behavior is consistent with previous studies [7].
- It is observed from Fig.8(b) that the settling time of the oscillations decreases as BWcc/BWvc increases. Low BWcc/BWvc ratios in the high distance - low power scenario values result in significant settling times, i.e. dc-link voltage oscillation can persist for seconds.
- The natural frequency shown in Fig.8(c) trend to decrease as the BWcc/BWvc ratio increases, but differences by a factor of 2 can be observed depending on the scenario. The frequency of the LFO might need be considered if control strategies aimed to cancel LFO are to be implemented [12].

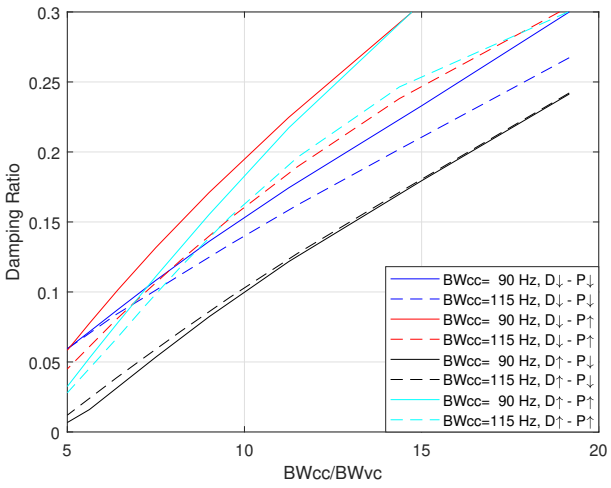

(a) Damping ratio vs. BWcc/BWvc

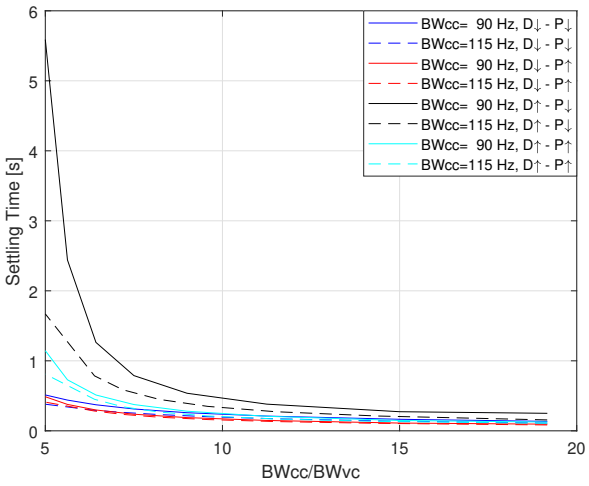

(b) Settling Time vs. BWcc/BWvc

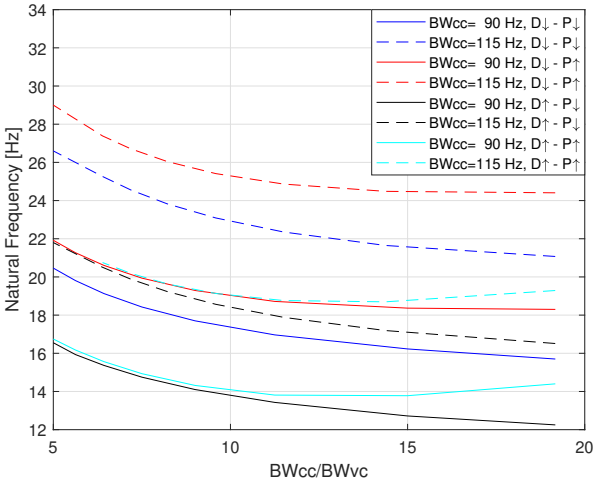

(c) Natural Frequency vs. BWcc/BWvc

Fig. 8: Damping ratio, Settling Time and Natural Frequency as a function of BWcc/BWvc ratio for different current control bandwidths (90 Hz and 115 Hz). D↓ and D↑ stands for low (20 km) and high distance (120 km), P↓ and P↑ stands for low and high power respectively

D. Eigenvalue migration with PLL and SOGI tuning

In addition to the control bandwidths and catenary distance discussed previously, other elements involved in the control of the 4QC might influence the LFO. These can include the PLL used to synchronize the 4QC with the catenary ac voltage, and the SOGI (depending on the control strategy being used).

Fig.9 shows the eigenvalue migration for variations in gains Kv_{sogi} and Ki_{sogi} of voltage and current SOGI. The gains are varied within a range of 0.7 to 1.3 or their nominal values, $Kv_{sogi-nominal} = 0.8$ and $Ki_{sogi-nominal} = 1$ respectively. Increasing Kv_{sogi} migrates system eigenvalues towards instability limit (i.e. shorter damping ratio), while increasing Ki_{sogi}, migrate the eigenvalues away from stability limit (i.e. larger damping ratio). However, increasing Ki_{sogi} implies an increasing of its bandwidth, which could compromise SOGI low-pass filter characteristic. It is concluded that a trade-off is required, sensitivity analysis of SOGI is performed in section IV-F.

Fig.10 shows eigenvalue migration for variations in gain K_{pll}. As mentioned in section II, the design of the PLL was performed according to [11] where the PLL proportional and integral gain are choosen as Kp_{pll}=K_{pll}, Ki_{pll}=$K_{pll}^2/2$. Generally speaking, PLL was found to have a marginal impact. Increasing K_{pll} by a factor as large as ten is seen to have a marginal effect on the eigenvalues. A sensitivity of PLL is performed in section IV-F.

E. Eigenvalue migration due to the leakage inductance (L_n) of transformer and dc-link capacitor (C_d)

Fig.11 shows the eigenvalue migration as a function of leakage inductance of transformer and dc-link capacitor. From this figure, it is possible to see that larger values of capacitance and inductance of the transformer improve stability against LFO. However, bigger capacitors are bulky and expensive, what places obvious constraints on the values that could be used. Also, designing a transformer to get a larger value of leakage inductance could limit the power transfer capability. Finally, from Fig.11, close to the stability limit, low values of the leakage inductance might provoke oscillations at lower frequencies than low values of the DC-Link capacitance. The trajectory of the eigenvalue migration of Cd tends to go to stability limit meanwhile increasing the oscillation frequency.

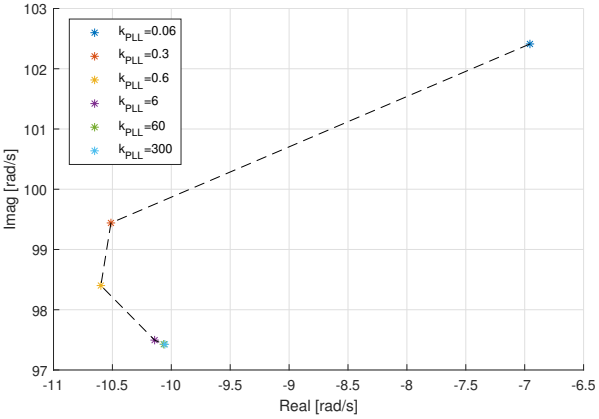

Fig. 10: Eigenvalue migration for variations in gain K_{pll}

F. Combined sensitivity analysis

A different approach to analyze the sensitivity to system parameters discussed in the previous subsections is to obtain the variation of the eigenvalues to an incremental variation of a given parameter, with the rest of system parameters remaining constant.

Fig.12 shows the variation of damping ratio, settling time and natural frequency, which results from this analysis. The analysis is performed for the case of of a catenary length of 120 km and a power consumption of 300 kW. The system is in this case close to the stability limit. System parameters being considered are changed within a range of 0.8 to 1.2 of their nominal value.

From Fig.12 the magnitude of the slope of each curve at the operational point (O.P) gives the sensitivity of the damping ratio, settling time and natural frequency to variation in the

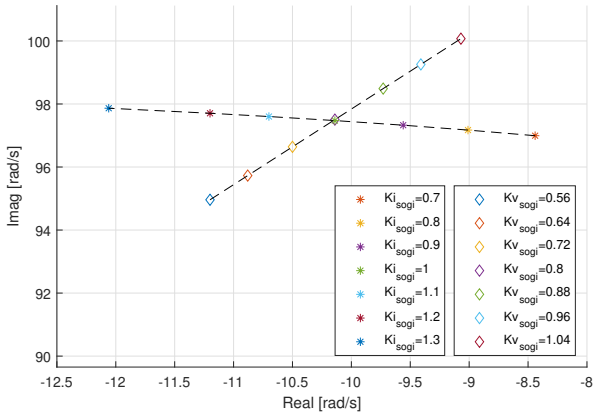

Fig. 9: Eigenvalue migration for variations in gains Kv_{sogi} and Ki_{sogi} correspond to voltage and current quadrature signal generator SOGI.

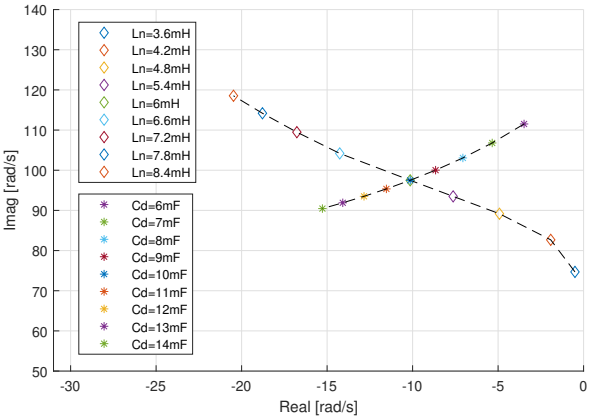

Fig. 11: Eigenvalue migration as a function of leakage inductance of transformer and dc-link capacitor

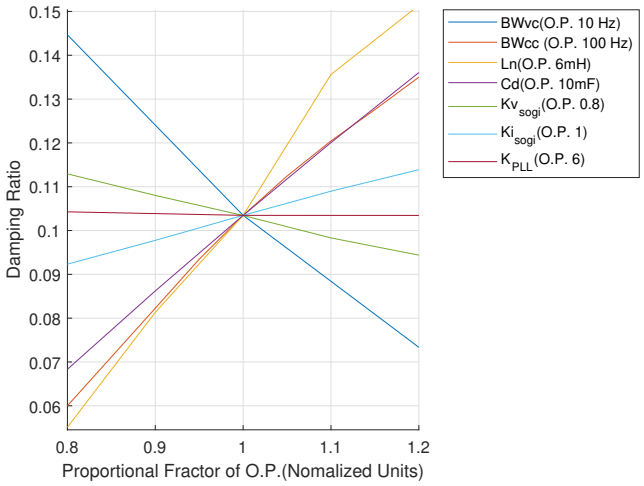

(a) Damping ratio vs. Proportional Factor (Normalized Units)

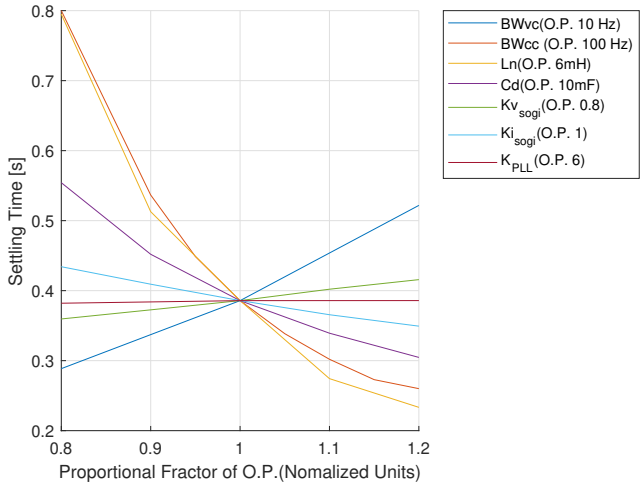

(b) Settling Time vs. Proportional Factor (Normalized Units)

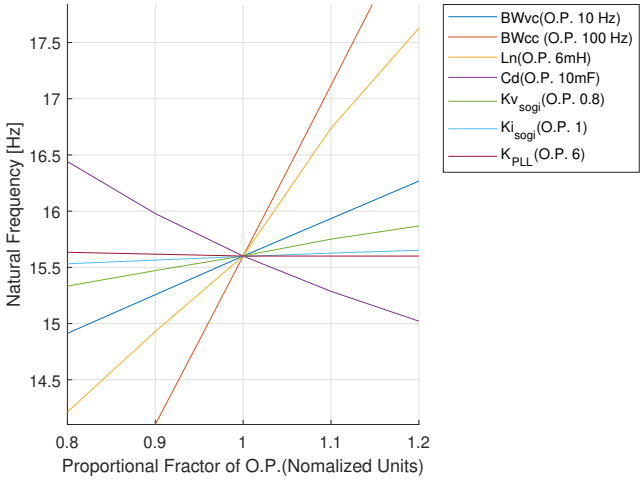

(c) Natural Frequency vs. Proportional Factor (Normalized Units)

Fig. 12: Damping ratio, Settling Time and Natural Frequency as a function of proportional factor of O.P.

proportional factor. For the damping ratio, positive slopes indicate that the system becomes more stable as the parameter being consider increases, the contrary occurs for negative slopes. Same reasoning applies for the setting time and natural frequency.

TABLE II: Sensitivity of dynamic system characteristics at O.P. Arrows ↑ and ↓ stands for positive sensitivity and negative sensitivity. Number of arrows show the degree of sensitivity.

	Damping R.(ζ)	Settling T.(T_s)	Natural Freq. (ω_n)
BWvc	↓↓	↑↑	↑↑
BWcc	↑↑	↓↓	↑↑↑
L_n	↑↑↑	↓↓↓	↑↑↑
C_d	↑↑	↓↓	↓↓
Kv_{sogi}	↓	↑	↑
Ki_{sogi}	↑	↓	↑
K_{pll}	-	-	-

Table II summarizes the results shown in Fig.12. It is observed that for the operating point being considered, LFO show highly sensitive to L_n and control bandwidths, while sensitivity to SOGI parameters is low, practically no sensitivity to PLL tuning is observed.

It is interesting to note that increasing the voltage-control bandwidth decreases the damping of the system, while increasing the current-control bandwidth, increases the damping of the system. Rather than the absolute values of the current and voltage control bandwidths, the system response is primarily given by the ratio BWcc/BWvc. This goes in accordance the analysis presented in section IV-C. It is concluded that low values of BWcc/BWvc significantly increase the risk of LFO.

Finally, it is noted that the trajectories shown in Fig. 12 and not necessarily straight lines. This is due to the non-linear nature of the system. This suggest that parameter sensitivity will depend on the operating point, this is a subject of ongoing research.

V. Conclusions

Time-domain simulation combined with eigenvalue migration analysis is proposed in this paper for the analysis of LFO phenomena in AC railway systems. The proposed method allows an insightful visualization of the sensitivity of LFO to catenary and train parameters, and consequently identifying critical modes of operation, as well as to propose remedial actions. It is concluded from the analysis performed in this paper that the worst scenario for LFO stability occurs for the case of trains operating far from substation and with low-power consumption. Catenary inductance (i.e. infrastructure parameter) and BWcc/BWv ratio (i.e. AFE control parameters) are the main two factors affecting to system stability.

References

[1] S. Menth and Meyer.M., "Low frequency power oscillations in electric railway systems," *eb - Elektrische Bahnen*, vol. 104, pp. 216–221, 2006.

[2] Y. Liao, Z. Liu, H. Zhang, and B. Wen, "Low-frequency stability analysis of single-phase system with dq-frame impedance approach—part i: Impedance modeling and verification," *IEEE Transactions on Industry Applications*, vol. 54, no. 5, pp. 4999–5011, 2018.

[3] L. Buhrkall, S. Danielsen, A. Eisele, M. Bergman, and J. Galic, "Low-frequency oscillations in scandinavian railway power supply - part i: Basic considerations," *eb - Elektrische Bahnen*, vol. 108, pp. 56–64, 01 2010.

[4] J. Suarez, P. Ladoux, N. Roux, H. Caron, and E. Guillame, "Measurement of locomotive input admittance to analyse low frequency instability on ac rail networks," in *2014 International Symposium on Power Electronics, Electrical Drives, Automation and Motion*, 2014, pp. 790–795.

[5] S. Danielsen, M. Molinas, T. Toftevaag, and O. Fosso, "Constant power load characteristic's influence on the low-frequency interaction between advanced electrical rail vehicle and railway traction power supply with rotary converters," 01 2009.

[6] H. Wang, W. Mingli, and J. Sun, "Analysis of low-frequency oscillation in electric railways based on small-signal modeling of vehicle-grid system in dq frame," *IEEE Transactions on Power Electronics*, vol. 30, no. 9, pp. 5318–5330, 2015.

[7] H. Hu, H. Tao, F. Blaabjerg, X. Wang, Z. He, and S. Gao, "Train–network interactions and stability evaluation in high-speed railways–part i: Phenomena and modeling," *IEEE Transactions on Power Electronics*, vol. 33, no. 6, pp. 4627–4642, 2018.

[8] H. Hu, H. Tao, X. Wang, F. Blaabjerg, Z. He, and S. Gao, "Train–network interactions and stability evaluation in high-speed railways—part ii: Influential factors and verifications," *IEEE Transactions on Power Electronics*, vol. 33, no. 6, pp. 4643–4659, 2018.

[9] S. Danielsen, "Ph.d. thesis: Electric traction power system stability: Low-frequency interaction between advanced rail vehicles and a rotary frequency converter," 2010.

[10] A. Yazdani and R. Iravani, *Voltage-Sourced Converters in Power Systems*. John Wiley & Sons, Ltd, 2010.

[11] S. Golestan and J. M. Guerrero, "Conventional synchronous reference frame phase-locked loop is an adaptive complex filter," *IEEE Transactions on Industrial Electronics*, vol. 62, no. 3, pp. 1679–1682, 2015.

[12] L. Buhrkall, S. Danielsen, A. Eisele, M. Bergman, and J. Galic, "Low-frequency oscillations in scandinavian railway power supply -part 2: Test of traction units," vol. 108, pp. 103–111, 03 2010.